ACS APPLIED MATERIALS & INTERFACES

Research Article

www.acsami.org

Solvothermal-Induced 3D Macroscopic SnO_2/Nitrogen-Doped Graphene Aerogels for High Capacity and Long-Life Lithium Storage

Ronghua Wang, Chaohe Xu, Jing Sun,* Lian Gao, and Heliang Yao

The State Key Lab of High Performance Ceramics and Superfine Microstructure, Shanghai Institute of Ceramics, Chinese Academy of Sciences, 1295 Ding Xi Road, Shanghai 200050, China

Supporting Information

ABSTRACT: 3D macroscopic tin oxide/nitrogen-doped graphene frameworks (SnO_2/GN) were constructed by a novel solvothermal-induced self-assembly process, using SnO_2 colloid as precursor (crystal size of 3−7 nm). Solvothermal treatment played a key role as N,N-dimethylmethanamide (DMF) acted both as reducing reagent and nitrogen source, requiring no additional nitrogen-containing precursors or post-treatment. The SnO_2/GN exhibited a 3D hierarchical porous architecture with a large surface area (336 m^2g^{-1}), which not only effectively prevented the agglomeration of SnO_2 but also facilitated fast ion and electron transport through 3D pathways. As a result, the optimized electrode with GN content of 44.23% exhibited superior rate capability (1126, 855, and 614 mAh g^{-1} at 1000, 3000, and 6000 mA g^{-1}, respectively) and extraordinary prolonged cycling stability at high current densities (905 mAh g^{-1} after 1000 cycles at 2000 mA g^{-1}). Electrochemical impedance spectroscopy (EIS) and morphological study demonstrated the enhanced electrochemical reactivity and good structural stability of the electrode.

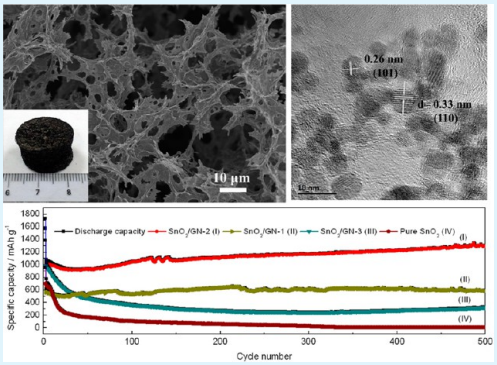

KEYWORDS: *tin oxide, solvothermal, nitrogen doping, graphene, aerogels, lithium ion batteries*

INTRODUCTION

Lithium ion batteries (LIBs) are currently the dominant power source for portable electronic devices and viewed as the most promising candidate to electrical/hybrid vehicles.[1,2] In order to store and transport energy more efficiently, many efforts have been devoted to explore various high-energy anode materials, such as SnO_2,[3,4] Fe_2O_3,[5] and Co_3O_4,[6] for the next generation of rechargeable LIBs. However, the practical use of these materials is greatly hampered by the poor cycling performance arising from their low electronic conductivity, severe aggregation, and huge volume changes upon extended Li insertion/extraction. To address these problems, fabricating carbonaceous nanocomposites, especially graphene-based hybrid anodes, was proved to be an effective strategy.[7−10] Graphene, with high conductivity and large specific surface area, can serve as an intriguing substrate to disperse electrochemically active materials, thus improving electrical conductivity and structural integrity of the electrode. To date, various graphene-based hybrid anodes have been developed. Although improved electrochemical performances have been achieved, some disadvantages for lithium storage still exist in these hybrids. For example, most of the previous works were focused on preparation of two-dimensional (2D) graphene-based composites in which nanoparticles anchored on the surface of graphene sheets (GS). In most cases, the 2D GS would easily reaggregate or restack during drying due to the van der Waals forces, which significantly reduced the accessible surface area and limited electron and ion transport.[2,11,12] Furthermore, GS usually possess a limited number of reactive sites, which result in a low specific capacity, large irreversible capacity, and fast capacity fade.[13−15] Therefore, it is still a big challenge to further optimize their electrochemical performance.

To overcome these issues, it is believed that two strategies are feasible. The first one is to assemble 2D GS into macroscopic 3D architectures, which can effectively prevent restacking of graphene, providing resultant graphene-based composites with large specific surface area, porous structure, and fast electron transport kinetics due to the continuous graphene backbone.[16−19] For example, Chen et al.[20]pioneered the capture of preprepared Fe_3O_4 into 3D graphene network under mild conditions (oil bath at 95 °C) with the aid of reducing agents ($NaHSO_3$). As claimed, the composite delivered a high capacity of 730 mAh g^{-1} even at a current density of 1600 mA g^{-1}. Similarly, Cong et al. developed α-FeOOH/GS and magnetic Fe_3O_4/GS hydrogels under the synergistic effects of the reduction of GO by ferrous ions and in situ simultaneous deposition of nanoparticles on GS.[21] Besides, MoS_2/GS,[18,22] Fe_2O_3/GS,[16,23] and TiO_2/GS[24] aerogels that were constructed by a hydrothermal method also demonstrated the effectiveness of macroscopic 3D architectures to the final lithium storage properties.

Received: December 5, 2013
Accepted: February 20, 2014
Published: February 20, 2014

 © 2014 American Chemical Society

Apart from the geometrical control, chemical doping, especially nitrogen-doping of GS, was another effective way to improve lithium storage performance.[14,15,25−27] This is because nitrogen doping can modulate the electronic structure of graphene, create defects to decrease the energy barrier of lithium penetration, and enhance reactive sites.[28,29] Very recently, a variety of transition metal oxides (e.g., TiO_2,[30,31] MnO,[32] Co_3O_4,[33] SnO_2,[28,34,35] Fe_2O_3[29]) composited with nitrogen-doped graphene (GN) have been designed as electrodes for LIBs. These hybrids exhibited significantly higher specific capacity than that of the metal oxide/GS counterpart. In this literature, either nitrogen-containing precursors (polypyrrole,[28] urea,[35,36] ammonia,[33] N_2H_4[31]) have to be added during the compositing process or additional post-treatment (N_2H_4 vapor treatment,[34] annealing in NH_3 atmosphere[30,32]) needs to be carried out for nitrogen-doping. For the former, the toxicity of the nitrogen source (N_2H_4, NH_3) should be considered, and the later often required rigorous conditions or special instruments. Therefore, it is still a challenge to prepare GN by a facile method. Considering that both nitrogen-doping of GS and 3D macroscopic frameworks can greatly improve lithium storage properties, it is highly demanded to develop graphene-based composites that combine the two characteristics together. However, to the best of our knowledge, little research has been done on this aspect.

In this study, we successfully constructed 3D macroscopic SnO_2/GN aerogels, comprising self-assembled nitrogen-doped graphene networks and ultrasmall SnO_2 nanocrystals (3−7 nm), via a novel solvothermal-induced self-assembly process using SnO_2 colloid sol as precursor. SnO_2 was selected as the research object because of its abundance and high theoretical capacity (782 mAh g^{-1} based on conventional alloying mechanism, 1494 mAh g^{-1} assuming that all Sn was oxidized to Sn^{4+}).[37,38] Here, solvothermal treatment played a key role as DMF acted both as reducing reagents and nitrogen sources, requiring no additional nitrogen-containing precursors or any post-treatment. The resulting macroscopic SnO_2/GN aerogels simultaneously possess high surface area (336 m^2 g^{-1}), hierarchical porous structure, and high electrical conductivity. Such unique features can facilitate the ultrafast diffusion of lithium ions/electrons within the electrode and, simultaneously, accommodate the volume change of SnO_2 during cycling. Moreover, nitrogen-doping of GS can modulate the electronic structure of graphene and further enhance the lithium storage properties. Benefitting from the combined N-doped property and 3D graphene frameworks, the SnO_2/GN exhibits excellent rate capability (1126, 855, and 614 mAh g^{-1} at 1000, 3000, and 6000 mA g^{-1}, respectively) and outstanding long-term cyclic stability at high current densities (905 mAh g^{-1} after 1000 cycles at 2000 mA g^{-1}). Importantly, the work described here can also be extended to prepare various metal oxide/GN aerogels, for the application in a broad range of LIBs, sensors, catalysts, and so on.

EXPERIMENTAL SECTION

Preparation of SnO_2 Nanocrystal Aqueous Dispersion. 1.0 g of $SnCl_4{\cdot}5H_2O$ was first dissolved in 50 mL of distilled water. The resulting solution was then hydrothermally treated at 120−180° C for 12−28 h. The obtained white precipitate was washed repeatedly by centrifugation and redispersed in water to form an aqueous dispersion.

Synthesis of SnO_2/GS Hybrid Aerogels. In a typical synthesis, SnO_2 dispersion was added dropwise into graphene oxide (GO) dispersion (2 mg mL^{-1}), followed by ultrasonicating for 30 min. The mixed suspension was centrifuged to remove H_2O and redispersed in 40 mL of DMF to form SnO_2/GO dispersion. Subsequently, SnO_2/GO dispersion in DMF was solvothermally treated at 120−200 °C for 6−16 h to reduce GO and induce self-assembly process to obtain a 3D SnO_2/GN monolith. Finally, the monolith was taken out, washed repeatedly with distilled water, and freeze-dried into an aerogel for further use. To obtain the optimal electrochemical performance, the various GN contents of 55.76%, 44.23%, and 18.62% were used. The samples were named as SnO_2/GN-1, SnO_2/GN-2, and SnO_2/GN-3, respectively. Detailed characterization was carried out on the optimized sample SnO_2/GN-2 hereafter.

Electrode Preparation. The electrodes were prepared by mixing 80 wt % active material, 10 wt % conducting carbon black, and 10 wt % polyvinylidene fluoride binder in N-methyl-2-pyrrolidone. The homogeneous slurries were then pasted on copper current collector and dried under vacuum at 110 °C for 12 h.

Material Characterization. The morphology of samples was characterized by the transmission electron microscope (JEM-2100F, JEOL, Tokyo, Japan). The field-emission scanning electron microscope (FE-SEM) analysis was performed on JSM-6700F at an acceleration voltage of 10.0 kV. X-ray diffraction (XRD) was carried out on D/max 2550 V X-ray diffraction-meter with Cu−Kα irradiation at λ = 1.5406. Thermal gravimetic analysis (TGA) was conducted in air at a heating rate of 10 °C min^{-1}. X-ray photoelectron spectroscopy (XPS) analysis was conducted using twin anode gun, Mg Kα (1253.6 eV) (Microlab 310F Scanning Auger Microprobe, VG SCIENTIFIC LTD). Conductivity was measured by a four-point probe method in the van der Pauw configuration with an Accent HL5500 system. N_2 adsorption/desorption isotherms were determined using a Micromeritics ASAP2010 Analyzer (USA).

Electrochemical Measurements. Cyclic voltammetry (CV) was carried out in a voltage range of 0−3.0 V with a scan rate of 0.5 mV s^{-1}. The electrochemical impedance spectroscopy (EIS) measurements were carried out with a PARSTAT 2273, using a sine wave of 10 mV over a frequency range of 100 kHz−0.1 Hz. The electrochemical properties of the electrodes were characterized at room temperature. Li foil was used as the counter electrode. The electrolyte was 1 M $LiPF_6$ in a 50:50 w/w mixture of ethylene carbonate (EC) and dimethyl carbonate (DMC). Cell assembly was carried out in a glovebox with the concentrations of moisture and oxygen below 1 ppm. The batteries were measured using a CT2001 battery tester.

RESULTS AND DISCUSSION

The SnO_2/GN 3D macroscopic aerogels were fabricated by a solvothermal-induced self-assembly strategy developed in our group and a subsequent freeze-drying process (Scheme 1). Briefly, homogeneous SnO_2 colloids were prepared using a hydrothermal method.[39] As is well known from colloidal science,[40] metal oxide colloid has a tendency to adsorb cations.

Scheme 1. Schematic Illustration of Preparation of SnO_2/GN Aerogels

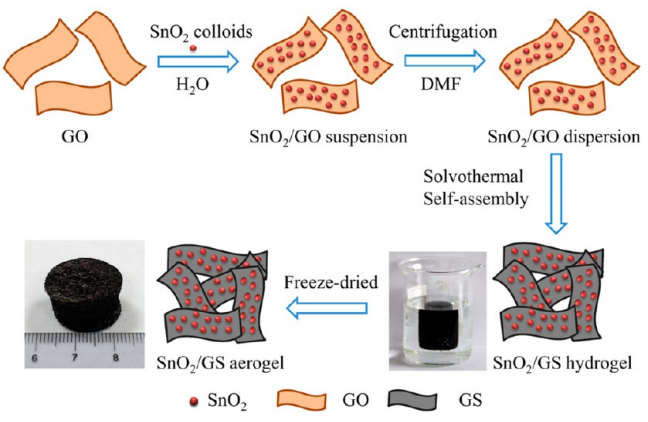

dx.doi.org/10.1021/am405557c | ACS Appl. Mater. Interfaces 2014, 6, 3427−3436

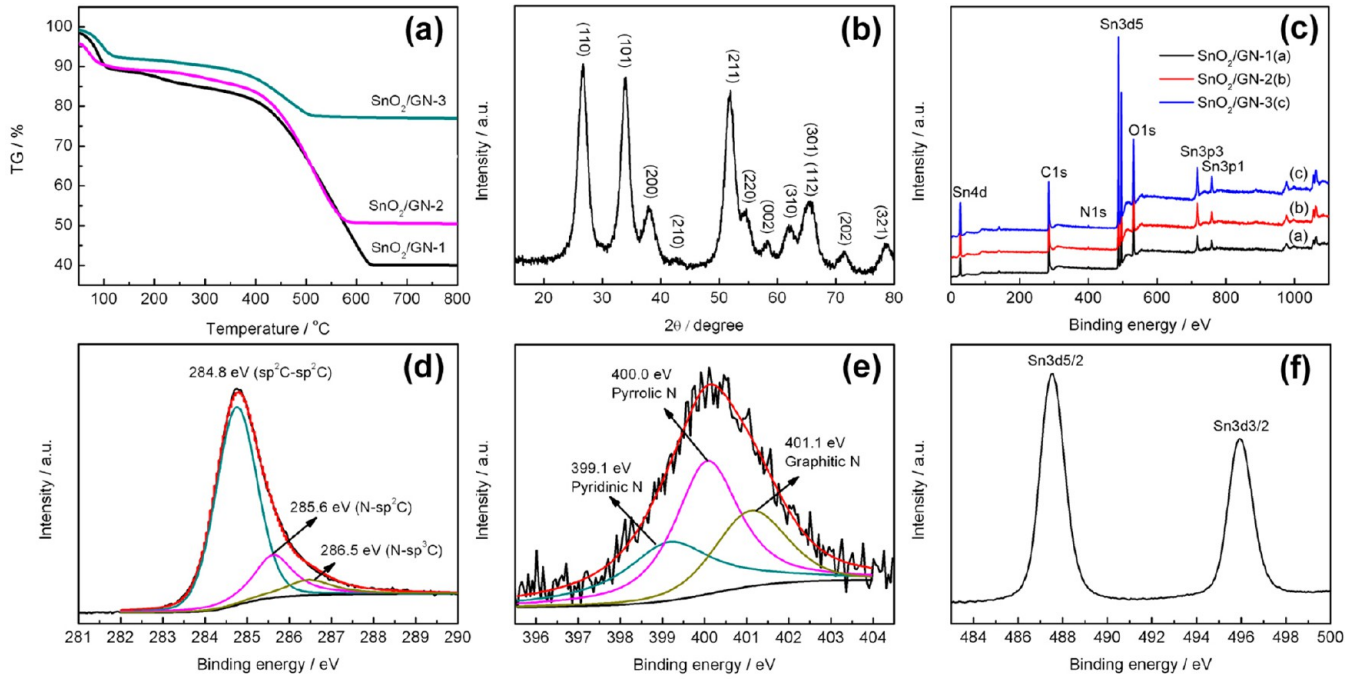

Figure 1. (a) TG curves and (b) XRD patterns of SnO_2/GN; (c) XPS spectra of SnO_2/GN; (d) XPS C1s spectrum of SnO_2/GN-2, which can be split into three peaks at 284.8, 285.8, and 286.5 eV; (e) XPS N1s spectrum of SnO_2/GN-2. The N1s peak can be split into three peaks at 399.1, 400.0, and 401.1 eV; (f) XPS Sn3d spectrum.

Here, the prepared SnO_2 was positively charged with a zeta potential of +34 mV, while GO was negatively charged (zeta potential was −56 mV) due to the presence of oxygen-containing functional groups.[5] Driven by strong electrostatic attractive interaction, SnO_2 colloidal nanoparticles (see the Supporting Information, Figure S1), with a diameter of 3−7 nm, can uniformly and tightly anchor on the surface of GO when they were mixed together (Figure S2). Noteworthy, even after a long time of sonication, SnO_2 still strongly connected with GO, further demonstrating the strong interaction between them. Subsequently, solvothermal treatment in DMF was employed to induce the self-assembly process and achieve nitrogen-doping of GS, where DMF acted as both reducing reagent and nitrogen sources,[41,42] requiring no additional nitrogen-containing precursors or any post-treatment. Specifically, GO was deeply reduced to GS with simultaneous incorporation of nitrogen species into the graphene lattice. Meanwhile, GN anchored with SnO_2 nanoparticles acted as a building block and self-assembled into a 3D monolith (Scheme 1) with an interconnected network, driven by $\pi-\pi$ stacking interactions due to the decrease of oxygenated groups on graphene.[21,24] Furthermore, the SnO_2 nanoparticles anchored on GN can serve as the space to effectively avoid aggregation of the GN during reduction process. Finally, the monolith was repeatedly exchanged with distilled water and freeze-dried to obtain aerogels. Notably, the content of SnO_2 in the as-prepared architectures was readily tunable by simply adjusting the ratio of SnO_2 to GO during the synthesis process. As shown in Figure 1a, the weight ratios of GN are 55.76%, 44.23%, and 18.62% for SnO_2/GN-1, SnO_2/GN-2, and SnO_2/GN-3, respectively, by getting rid of the weight loss of adsorption water. Detailed calculation can be found in Figure S3. The conductivity of SnO_2/GN-2 was measured to be 97 S m^{-1}. It means GN can serve as an efficient electrically conducting network for fast electronic transport, which will result in high powder density of the electrode. XRD revealed that the peaks of SnO_2 in SnO_2/GN can be well indentified as a tetragonal rutile-like SnO_2 (Figure 1b, JCPDF 41-1445).

To confirm N-doping of graphene, X-ray photoemission spectroscopy (XPS) studies were carried out. The survey scan spectrum from XPS analysis showed the sample contained C, O, N, and Sn elements (Figure 1c). The atomic percentages of doped nitrogen in GN are 2.17%, 2.25%, and 2.22% for SnO_2/GN-1, SnO_2/GN-2, and SnO_2/GN-3, respectively. The C1s core level peak of SnO_2/GN-2 can be resolved into three components centered at 284.8, 285.6, and 286.5 eV, assigned to sp^2C-sp^2C, N-sp^2C, and N-sp^3C bonds,[7,43] respectively (Figure 1d). Similarly, the N1s peak can also be resolved into three components centered at 399.1, 400.0, and 401.1 eV, representing pyridinic, pyrrolic, and graphitic type of N atoms doped in the graphene structure[7,29] (Figure 1e). Nitrogen doping can introduce a large number of surface defects into graphene, which leads to the formation of a disordered carbon structure that enhances Li intercalation properties.[32,43] Additionally, theoretical studies illustrated that the pyridinic N in carbon materials could apparently reduce the energy barrier for Li penetrating (about 1.44 eV, much lower than that of 10.5 eV for perfect GS).[35,43,44] Since lithium storage is also a kinetic process, the existence of vacancies and electron deficiencies in pyridinic N will provide a feasible pathway for Li penetration into graphene layers, thus also contributing to the improvement of reversible capacity. In addition, the Sn3d5/2 (487.2 eV) and Sn3d3/2 (495.6 eV) peaks found in the XPS data (Figure 1f) further confirm the formation of SnO_2.

The morphology and structure of the resultant SnO_2/GN were characterized by FE-SEM and TEM (Figure 2). SEM images showed an interconnected, porous 3D graphene framework with continuous macropores in the micrometer size range (Figure 2a and b). Closer observation discloses that

dx.doi.org/10.1021/am405557c | ACS Appl. Mater. Interfaces 2014, 6, 3427−3436

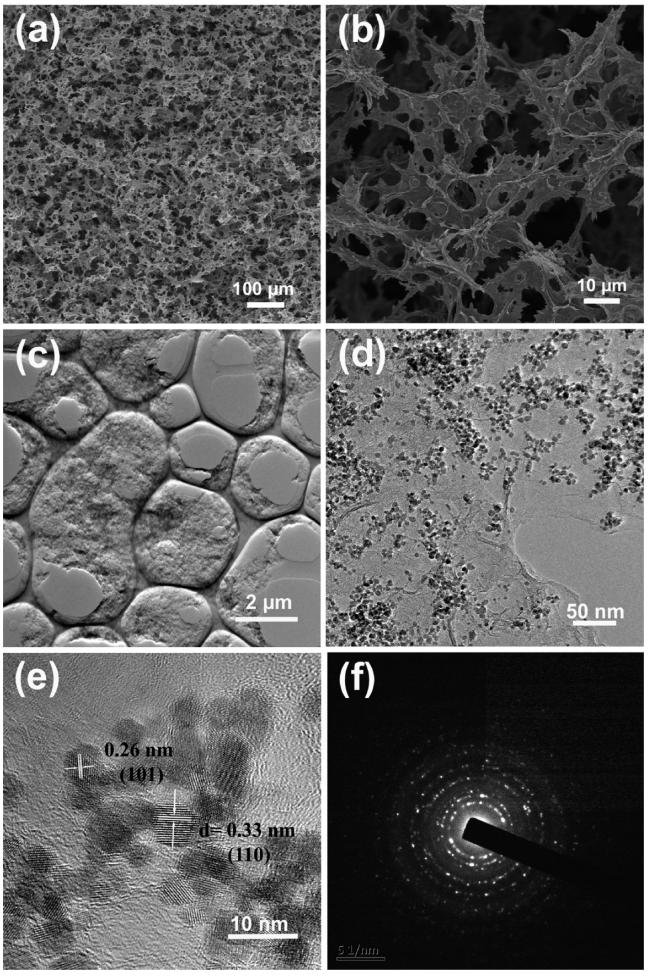

Figure 2. The morphology and nanostructure of the resultant SnO_2/GN-2: (a-b) SEM images, (c-d) TEM images, (e) HRTEM image, and (f) the corresponding SAED patterns.

SnO_2 nanoparticles, with a particle size of 3−7 nm, were homogeneously dispersed within the hybrid (Figure S4). The chemical composition was verified by energy dispersive spectroscopy (EDS) where elements Sn, O, and C were detected (Figure S5). A low-magnified TEM image of SnO_2/GN (Figure 2c) showed that the size of GN was about several micrometers, while the high-magnified TEM image further demonstrated that SnO_2 nanocrystals were homogeneously distributed on the surface of GN (Figure 2d), consistent well with SEM images. The HRTEM image displayed that SnO_2 was highly crystalline with crystal lattice fringes of 0.33 and 0.26 nm (Figure 2e), corresponding to the (110) and (101) face of SnO_2, respectively. The corresponding selected area electron diffraction (SAED) pattern further demonstrated the high-quality single-crystalline nature of SnO_2.

The porous nature of SnO_2/GN-2 architecture was demonstrated by BET measurement (Figure 3). The adsorption-desorption isotherms exhibited a typical IV hysteresis loop at a relative pressure between 0.4 and 0.8, characteristic of pores with different pore sizes (Figure 3a). Remarkably, the specific surface area of SnO_2/GN-2 reached up to 336 $m^2\ g^{-1}$, which was much higher than that of pure SnO_2 (176 $m^2\ g^{-1}$). This result highlighted that the building up of 3D frameworks by solvothermal assembly was an effective way to achieve a high surface area for hybrid materials.[16,22] BJH calculations disclosed the pore volume was 0.234 $cm^3\ g^{-1}$ with an average pore diameter of 3.7 nm (the inset in Figure 3a). The high porosity can provide not only more surface reaction sites but also sufficient buffer space to alleviate the volume expansion of SnO_2 during lithiation and delithiation and is therefore favorable for the electrochemical properties.[2,25]

Coin cells with metallic Li counter electrode were assembled to evaluate the electrochemical performance of the electrode. Figure 4a exhibited the CV curves for the first five cycles of the SnO_2/GN-2 electrode. In the first cathodic scan, there are four reduction peaks at 1.27 V, 0.85 V, ∼0.6 V, and ∼0.1 V, respectively. The two at 1.27 and 0.85 V should be attributed to the reduction of SnO_2 to SnO (eq 1), the conversion of SnO to Sn (eq 2), respectively, accompanying with the formation of Li_2O.[45] The shoulder peak at ∼0.6 V can be ascribed to the decomposition of the electrolyte on the surface of SnO_2 and GN, leading to the formation of the solid-electrolyte-interphase (SEI).[34] The fourth reduction peak around 0.1 V reflects Li−Sn alloying (eq 3) and the intercalation of lithium ion into GN (eq 4).[45,46] In the first anodic process, the oxidation peak at 0.58 V was related to the dealloying of Li*x*Sn (eq 3). While another peak at 1.29 V was ascribed to partial transformation of Sn and Li_2O to SnO_2.[34,38,47,48] This indicated that the commonly regarded irreversible conversion reaction, $SnO_2 + 4Li^+ + 4e^- \rightarrow 2Li_2O + Sn$, was partial reversible in SnO_2/GN composite (eqs 1 and 2). It was well known that the required activation energy for oxidation and solid-state double decomposition reactions decreased with decreasing particle size.[37,49] Here, the reversible conversion reaction of SnO_2 may be due to the ultrasmall size of SnO_2.[50] In the subsequent cycles, the CV curves were almost

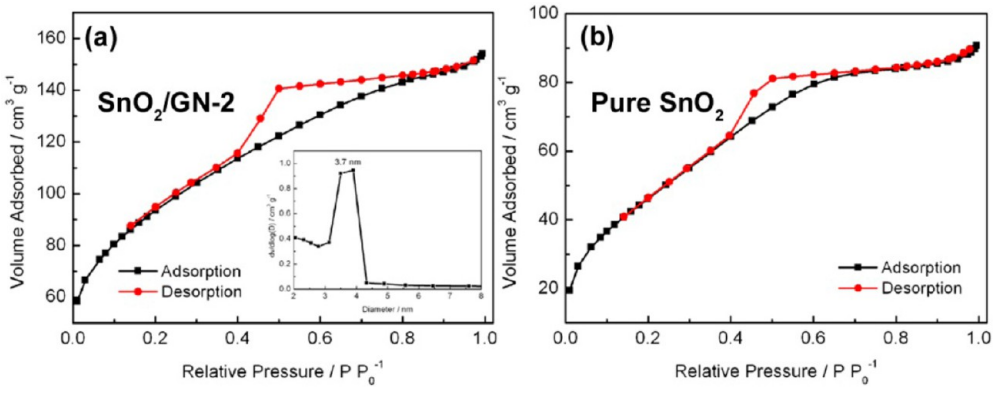

Figure 3. Nitrogen adsorption and desorption isotherms of SnO_2/GN-2 (a) and pure SnO_2 (b).

dx.doi.org/10.1021/am405557c | ACS Appl. Mater. Interfaces 2014, 6, 3427−3436

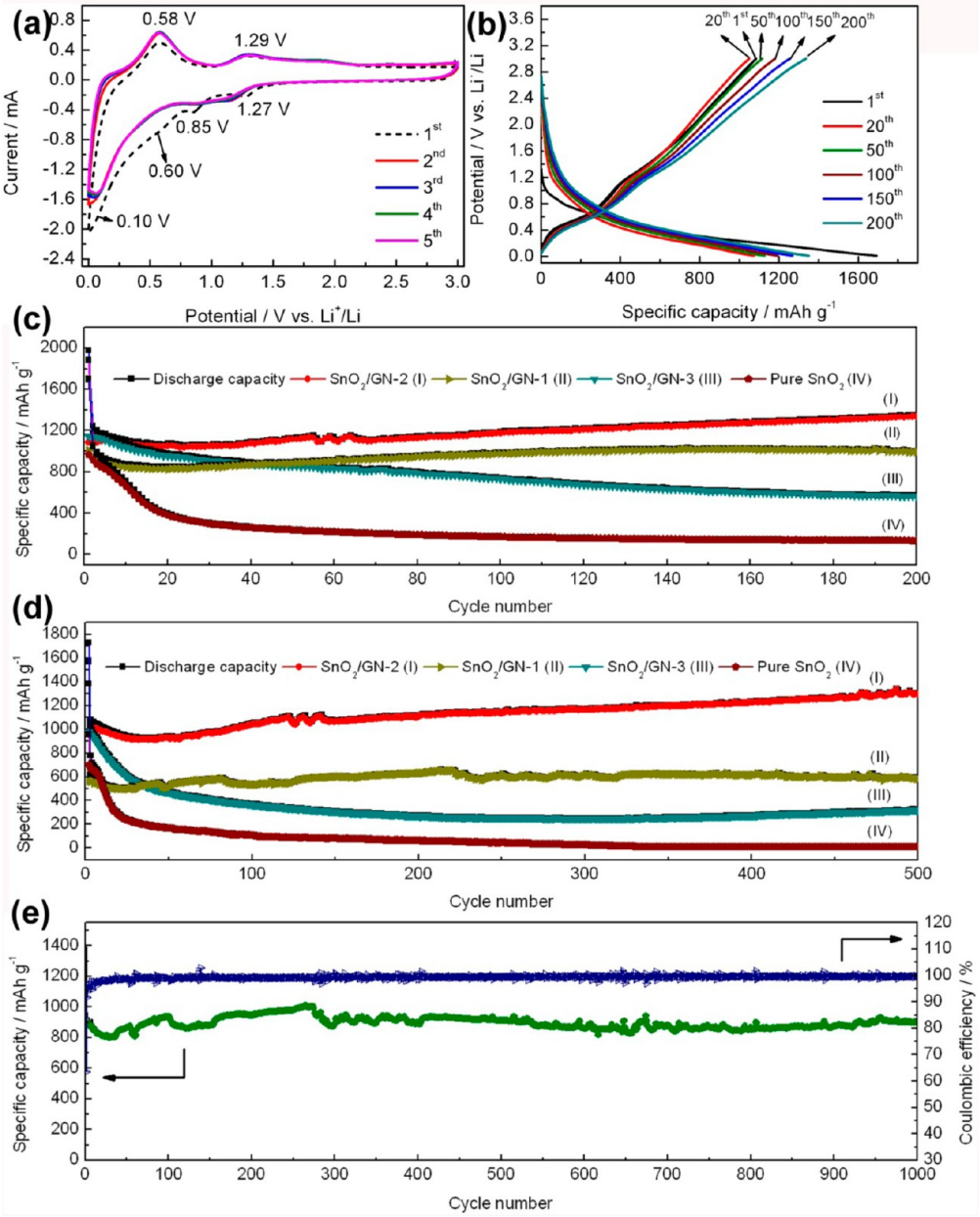

Figure 4. (a) Cyclic voltammograms for the first five cycles of SnO_2/GN-2 electrode; (b) charge-discharge profiles of SnO_2/GN-2 electrode at a current density of 500 mA g^{-1}; (c and d) comparative cycle performance of different electrodes at a current density of 500 and 1000 mA g^{-1}, respectively; (e) cycle performance of SnO_2/GN-2 electrode at a current density of 2000 mA g^{-1}. The capacity is based on the weight of the whole composite.

overlapped, implying an excellent reversibility of lithium insertion and extraction reactions. The whole process can be expressed as

$$SnO_2 + 2Li^+ + 2e^- \leftrightarrow SnO + Li_2O \quad (1)$$

$$SnO + 2Li^+ + 2e^- \leftrightarrow Sn + Li_2O \quad (2)$$

$$Sn + xLi^+ + xe^- \leftrightarrow LixSn\ (0 \le x \le 4.4) \quad (3)$$

$$C(GN) + xLi^+ + xe^- \leftrightarrow LixC \quad (4)$$

Figure 4b showed the representative charge/discharge curves of SnO_2/GN-2 at a current density of 500 mA g^{-1} between 0.01−3.0 V vs Li^+/Li. A voltage plateau ranging from 0.6 to 1.4 V was observed at the discharge step, while two plateaus at ~0.6 and 1.3 V existed in the charge curves. The charge/discharge curves were in good accordance with the CV profiles. The initial discharge and charge capacity were 1693 and 1083 mAh g^{-1} (based on the total mass of SnO_2/GN hybrid material), respectively, corresponding to a coulombic efficiency (CE) of 64.0%. This performance is close to the theoretical capacity of SnO_2/GN-2[51,52,34,53] ($C_{theo.} = C_{SnO2,theo} \times \%_{SnO2} + C_{GS,theo} \times \%_{GS} = 1494 \times 0.5577 + 774 \times 0.4423 = 1175.5$ mAh g^{-1}). The ultrasmall size of SnO_2 nanocrystals, unique 3D porous architectures coupled with nitrogen-doping of graphene should contribute mostly to such high capacities. Specifically, on one hand, the SnO_2 in the GN matrix had a fine particle size (3−7 nm) and multiple electrical contacts with the carbon matrix, which endow the electrode superior electrochemical activities and large electrochemical interface lithium storage. On

dx.doi.org/10.1021/am405557c | ACS Appl. Mater. Interfaces 2014, 6, 3427−3436

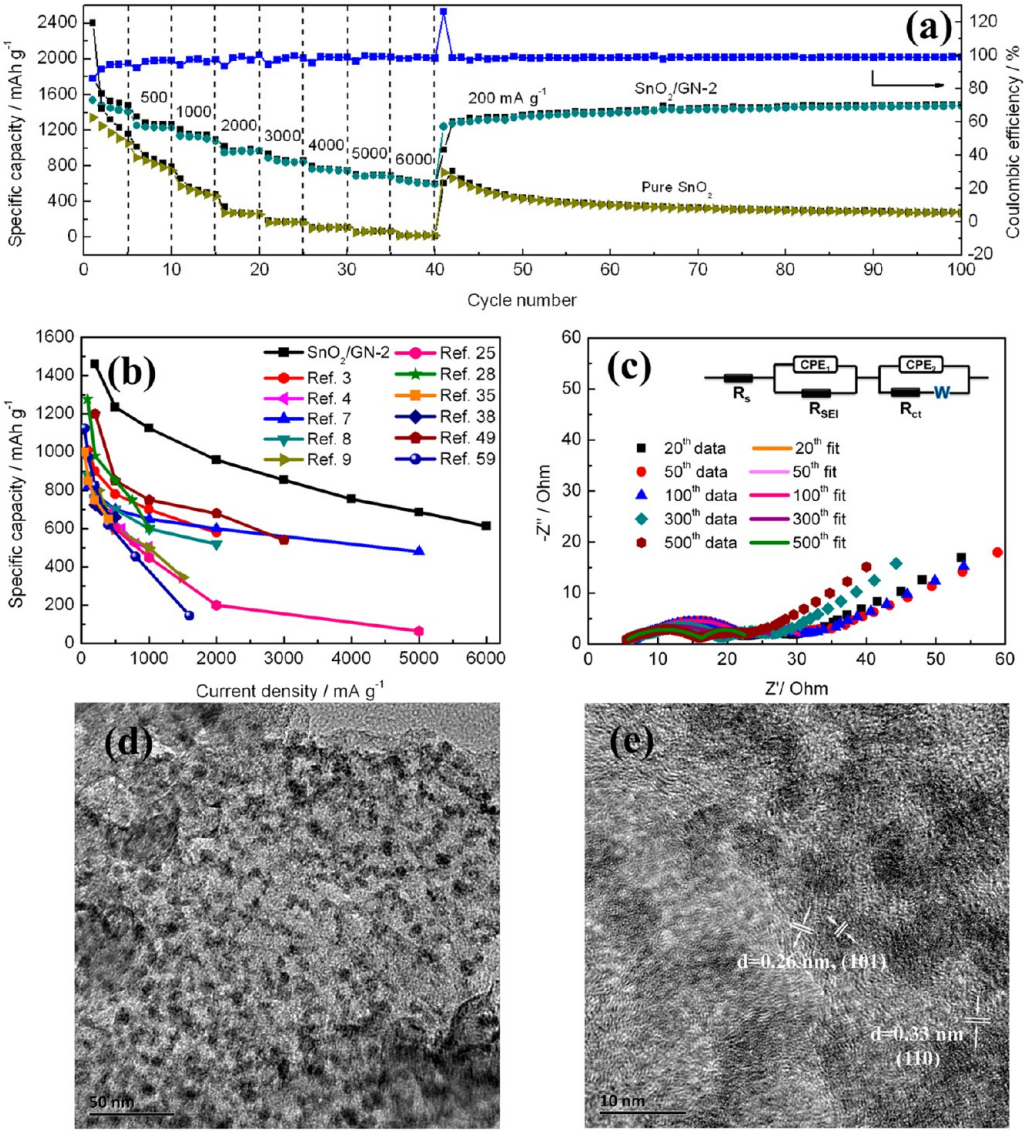

Figure 5. (a) The rate capability of SnO_2/GN-2 and pure SnO_2 electrode at different current densities (200-6000 mA g^{-1}); (b) Comparison of capacity at different current densities for SnO_2/GN-2 electrodes with those of reported SnO_2-based hybrid anodes; (c) Nyquist plots SnO_2/GN-2 after specific cycles. The inset in (c) represents the equivalent circuit model of the electrode. CPE is the constant phase element; (d and e) TEM and HRTEM images of SnO_2/GN-2 after cycling at 500 mA g^{-1}.

the other hand, the unique 3D porous architectures can facilitate fast ion and electron transport through 3D pathways and provide the electrode with abundant reactive sites.[54] Thirdly, graphene, especially nitrogen-doped graphene, with rich of sides and defects, can also greatly enhance the lithium storage capacity. Subsequently, the charge capacity slightly decreased during 20 cycles (1050 mAh g^{-1}) and then gradually increased in the following cycles and reached up to 1340 mAh g^{-1} after 200 cycles (capacity retention of 134%). The higher performance of SnO_2/GN-2 than that of theoretical capacity can be attributed to the very small size with large electrochemical interface lithium storage,[55,56] superior electrochemical activities, and also partial reversible reaction of the SEI.[19] Similar phenomenon, that capacity decreased to some extent then gradually increased, has been commonly observed in metal oxide/carbon composites.[2,37,49,57] Closer observation showed that the differences among the charge curves of different cycles mainly happened above 1.0 V (the oxidation of Sn). The slight decay of capacity during the first 20 cycles could be due to the partial pulverization of original SnO_2 and in situ formed Sn. As demonstrated in previous reports, the particle size of SnO_2 and Sn will become smaller than original ones due to electrochemical milling effect after continuous cycling.[37,53,58,59] Therefore, the reactivity of oxidation of Sn to SnO_2 will be enhanced due to the decreased particle size, which may result in the gradual increase in capacity after 20 cycles.

To understand the effect of the SnO_2/GN ratio on electrochemical performance, composites with different relative content of SnO_2 and GN were prepared (Figure 4c). The GN contents were 55.76%, 44.23%, and 18.62% for SnO_2/GN-1, SnO_2/GN-2, and SnO_2/GN-3 as determined by TG, respectively. For pure SnO_2, the capacity decayed severely and retained only 136 mAh g^{-1} after 200 cycles, with the capacity retention of 14%. It should be pointed that although conversion reaction was also partially reversible during the first several cycles, the plateau above 1.0 V completely disappeared after 15 cycles (Figure S6). This may due to the high volume variation of Sn (>300%) and severe agglomeration, which leads

to the cracking and pulverization of the electrode, as well as a loss of electrical contact between active Sn and conductive additives or current collector.[3,39] For SnO_2/GN-3, with the lowest amount of GN, serious capacity loss also occurred during cycling and retained only ~566 mAh g^{-1} after 200 cycles. This is because such low content of GN was inadequate to well disperse SnO_2 nanocrystals, which would also result in pulverization and rapid capacity fading.[2] On the other hand, the lower conductivity may be another reason for the capacity decrease. In the case of SnO_2/GN-2, SnO_2 was tightly attached to GN and spatially separated, which helped to accommodate the volume change and prevent aggregation. Therefore, the specific capacity is the highest and cycling performance is much better than that of SnO_2/GN-3. Further increasing the content of GN in the hybrid (SnO_2/GN-1), although good cycling stability was also achieved (~100% capacity retention), the capacity (998 mAh g^{-1}) was much lower than that of SnO_2/GN-2. Here, SnO_2/GN-2 represented the highest specific capacity and the best cycling stability.

To further demonstrate the extraordinary cyclic stability of SnO_2/GN-2, the electrode was tested at a higher current density of 1000 mA g^{-1} with a larger numbers of cycles (Figure 4d). Similarly, SnO_2/GN-2 exhibited the best cyclic performance: a capacity as high as 1305 mAh g^{-1} was delivered after 500 cycles with a capacity retention of 136.7%. Even at an ultrahigh current density of 2000 mA g^{-1}, SnO_2/GN-2 still possessed a capacity up to 905 mAh g^{-1} after 1000 cycles with a capacity retention of 102%, demonstrating an excellent prolonged cycling stability. Additionally, the average coulombic efficiency achieved nearly ~100% from the second cycle, indicating stabilization of SEI.[1,6] Recently, Xu et al. reported a specific capacity of 1182 mAh g^{-1} at a current density of 100 mA g^{-1} for SnO_2 nanorods dispersed GN, which decreased to 803 mAh g^{-1} after 100 cycles.[35] Wang et al. showed a specific capacity of 910 mAh g^{-1} at 50 mA g^{-1} for GN-SnO_2 sandwich paper.[7] In another report, Ramaprabhu and co-workers synthesized SnO_2 nanoparticles dispersed GN, which delivered a capacity of 793 mAh g^{-1} after 100 cycles at 90 mA g^{-1}.[28] Thus, the present SnO_2/GN aerogel exhibited a higher capacity and superior cyclic stability as compared to previously reported SnO_2/GN composites.

Besides high capacity and excellent cycling stability, SnO_2/GN also displayed superior rate capability. As shown in Figure 5a, the hybrid electrode delivered very high capacities of 1460, 1235, 1126, and 960 mAh g^{-1} at 200, 500, 1000, and 2000 mA g^{-1}, respectively. Even at ultrahigh current density of 3000, 4000, 5000, and 6000 mA g^{-1}, the electrode still retained capacities up to 855, 755, 686, and 614 mAh g^{-1}, respectively. This rate performance was quite remarkable in that the capacity of 616 mAh g^{-1} was achieved within ~6.0 min of charging or discharging time. Remarkably, the charge/discharge curves still maintained a kinetic feature at high current densities, indicating a facile charge transport process[1] (Figure S7). Noteworthy, few of the previously reported work have reported the rate performance under high current density of 6000 mA g^{-1}. Figure 5b reveals that the rate capability of SnO_2/GN-2 is higher than most of the reported SnO_2-based hybrid electrodes [SnO_2/GS (refs 3 and 8); SnO_2/GN (refs 7, 28, and 35); SnO_2/GS aerogel (ref 38); SnO_2@carbon (refs 4 and 59); GS/SnO_2/carbon (refs 25 and 49); SnO_2/GS/CNTs (ref 9)]. Importantly, a capacity of 1470 mAh g^{-1} can be recovered in another 60 cycles when the current density returned to 200 mA g^{-1}. This further implied the stable structure of the hybrid and the excellent reversibility. As demonstrated in previous study, the high rate performance was greatly dependent on the rapid ionic and electronic diffusion and transport. As for SnO_2/GN, the ultrasmall size of SnO_2 nanocrystals can dramatically shorten lithium diffusion length. The porous structure facilitated the penetration and diffusion of electrolyte, leading to fast lithium ion transport. Meanwhile, the interconnecting nitrogen-doped graphene network can provide 3D electron conducting channels within the electrode. In this way, both high speed electron and lithium ion pathways are satisfied. In contrast, pure SnO_2 exhibited poorer rate capability and cannot bear large current densities due to the inefficient ionic and electronic transport.

To explore the structural stability of the cycled electrode, we investigated the changes of morphology and structure of the electrode by using ex situ TEM technique. For pure SnO_2 electrode, Sn nanoparticles appear to aggregate into Sn clusters during cycling (Figure S8). These large Sn particles may not maintain their integrity due to the large volume change during cycling, resulting in poor capacity retention. In the case of SnO_2/GN electrode, it is clearly seen that the primary dispersibility was well preserved, demonstrating a good constraint on the aggregation of SnO_2 upon cycling (Figure 5d and e). The particles were pulverized into a smaller size of 3−5 nm, which is beneficial to lower the absolute volume change and achieve higher electrochemical reactivity, resulting in an enhanced capacity during cycling.[59,60] In the HRTEM image, the nanoparticles showed a poor crystallinity; however, lattice fringes of SnO_2 can also be observed, which further confirms that the conversion reaction of SnO_2 to Sn and Li_2O is reversible.

Furthermore, AC impedance analysis was carried out to elucidate the charge and contact resistance of SnO_2/GN and pure SnO_2 at selected cycle numbers. The high frequency semicircle is associated with SEI film resistance (R_{SEI}), the middle frequency semicircle is linked to charge-transfer resistance through the electrode-electrolyte interface (R_{ct}), while the steep sloping line represents the lithium-diffusion process within electrodes.[38,61,62] For pure SnO_2, R_{SEI} and R_{ct} increased dramatically with cycling, implying continuous growth of the SEI film and degraded charge transfer kinetics[63,64] (Figure S9). In contrast, SnO_2/GN displayed a drastically smaller diameter of both semicircles than that of pure SnO_2 after the same cycles, benefitting from the highly conductive graphene network (Figure 5c). EIS fitting showed that R_{SEI} and R_{ct} decreased upon cycling (Table S1), demonstrating stable SEI and increased electron and lithium ion diffusion rate, which results from the reduced size of Sn and SnO_2 nanoparticles.[49,65] Due to the excellent structural stability as well as facilitated transportation of electrons and lithium ions, SnO_2/GN exhibits both superior cycling and rate performances.

CONCLUSIONS

We have successfully constructed 3D macroscopic SnO_2/GN aerogels, comprising self-assembled nitrogen-doped graphene networks and ultrasmall SnO_2 nanocrystals (3−7 nm), via a novel solvothermal-induced self-assembly process using SnO_2 colloid sol as precursor. Such a unique architecture established by GN prevents the electrochemical aggregation of SnO_2 and ensures favorable transport kinetics for both electrons and lithium ions. Moreover, nitrogen-doping of GS can further modulate the electronic structure of graphene and further enhance the lithium storage properties. Benefitting from the

combined 3D graphene frameworks and nitrogen-doping effect, extraordinary rate capability and prolonged cyclic stability (905 mAh g^{-1} after 1000 cycles at 2000 mA g^{-1}) were achieved. Morphological and EIS study demonstrated the persistent uniform distribution of SnO_2 and increased electrochemical reactivity of the electrode during cycling. We believe that the present synthetic route can be further extended to produce other graphene-based hybrid aerogels, for applications in catalysts, sensors, supercapacitors, and so on.

■ ASSOCIATED CONTENT

Supporting Information

Additional TEM, SEM, TG, EDS, CV, discharge−charge curves, EIS curves, and photograph of SnO_2 dispersion. This material is available free of charge via the Internet at http://pubs.acs.org.

■ AUTHOR INFORMATION

Corresponding Author

*Phone: +86 21 52414301. Fax: +86 21 52413122. E-mail: jingsun@mail.sic.ac.cn.

Notes

The authors declare no competing financial interest.

■ ACKNOWLEDGMENTS

This work is supported by the 973 Project (2012CB932303), the National Natural Science Foundation of China (Grant No. 50972153, 51072215, and 51172261).

■ REFERENCES

(1) Jia, X. L.; Chen, Z.; Cui, X.; Peng, Y. T.; Wang, X. L.; Wang, G.; Wei, F.; Lu, Y. F. Building Robust Architectures of Carbon and Metal Oxide Nanocrystals toward High-Performance Anodes for Lithium-Ion Batteries. *ACS Nano* **2012**, *6*, 9911−9919.

(2) Wang, R. H.; Xu, C. H.; Sun, J.; Gao, L.; Lin, C. C. Flexible Free-Standing Hollow Fe_3O_4/Graphene Hybrid Films for Lithium-Ion Batteries. *J. Mater. Chem. A* **2013**, *1*, 1794−1800.

(3) Lin, J.; Peng, Z. W.; Xiang, C. S.; Ruan, G. D.; Yan, Z.; Natelson, D.; Tour, J. M. Graphene Nanoribbon and Nanostructured SnO_2 Composite Anodes for Lithium Ion Batteries. *ACS Nano* **2013**, *7*, 6001−6006.

(4) Zhang, L.; Zhang, G. Q.; Wu, H. B.; Yu, L.; Lou, X. W. Hierarchical Tubular Structures Constructed by Carbon-Coated SnO_2 Nanoplates for Highly Reversible Lithium Storage. *Adv. Mater.* **2013**, *25*, 2589−2593.

(5) Du, M.; Xu, C. H.; Sun, J.; Gao, L. Synthesis of α-Fe_2O_3 Nanoparticles from $Fe(OH)_3$ Sol and Their Composite with Reduced Graphene Oxide for Lithium Ion Batteries. *J. Mater. Chem. A* **2013**, *1*, 7154−7158.

(6) Sun, J.; Wang, R. H.; Xu, C. H.; Liu, Y. Q.; Gao, L.; Lin, C. C. Free-Standing and Binder-Free Lithium-Ion Electrode Based on Robust Layered Assembly of Graphene and Co_3O_4 Nanosheets. *Nanoscale* **2013**, *5*, 6960−6967.

(7) Wang, X.; Cao, X. Q.; Bourgeois, L.; Guan, H.; Chen, S. M.; Zhong, Y. T.; Tang, D. M.; Li, H. Q.; Zhai, T. Y.; Li, L.; Bando, Y.; Golberg, D. N-Doped Graphene-SnO_2 Sandwich Paper for High-Performance Lithium-Ion Batteries. *Adv. Funct. Mater.* **2012**, *22*, 2682−2690.

(8) Prabakar, S. J. R.; Hwang, Y. H.; Bae, E. G.; Shim, S.; Kim, D.; Lah, M. S.; Sohn, K. S.; Pyo, M. SnO_2/Graphene Composites with Self-Assembled Alternating Oxide and Amine Layers for High Li-Storage and Excellent Stability. *Adv. Mater.* **2013**, *25*, 3307−3312.

(9) Zhang, B. A.; Zheng, Q. B.; Huang, Z. D.; Oh, S. W.; Kim, J. K. SnO_2-Graphene-Carbon Nanotube Mixture for Anode Material with Improved Rate Capacities. *Carbon* **2011**, *49*, 4524−4534.

(10) Wang, L.; Wang, D.; Dong, Z.; Zhang, F.; Jin, J. Interface Chemistry Engineering for Stable Cycling of Reduced GO/SnO_2 Nanocomposites for Lithium Ion Battery. *Nano Lett.* **2013**, *13*, 1711−1716.

(11) Luo, J. Y.; Jang, H. D.; Sun, T.; Xiao, L.; He, Z.; Katsoulidis, A. P.; Kanatzidis, M. G.; Gibson, J. M.; Huang, J. X. Compression and Aggregation-Resistant Particles of Crumpled Soft Sheets. *ACS Nano* **2011**, *5*, 8943−8949.

(12) Luo, J. Y.; Jang, H. D.; Huang, J. X. Effect of Sheet Morphology on the Scalability of Graphene-Based Ultracapacitors. *ACS Nano* **2013**, *7*, 1464−1471.

(13) Mou, X.; Zhang, B.; Li, Y.; Yao, L.; Wei, X.; Su, D. S.; Shen, W. Rod-Shaped Fe_2O_3 as an Efficient Catalyst for the Selective Reduction of Nitrogen Oxide by Ammonia. *Angew. Chem., Int. Ed.* **2012**, *51*, 2989−2993.

(14) Wang, H. B.; Zhang, C. J.; Liu, Z. H.; Wang, L.; Han, P. X.; Xu, H. X.; Zhang, K. J.; Dong, S. M.; Yao, J. H.; Cui, G. L. Nitrogen-Doped Graphene Nanosheets with Excellent Lithium Storage Properties. *J. Mater. Chem.* **2011**, *21*, 5430−5434.

(15) Li, X. F.; Geng, D. S.; Zhang, Y.; Meng, X. B.; Li, R. Y.; Sun, X. L. Superior Cycle Stability of Nitrogen-Doped Graphene Nanosheets As Anodes for Lithium Ion Batteries. *Electrochem. Commun.* **2011**, *13*, 822−825.

(16) Xiao, L.; Wu, D. Q.; Han, S.; Huang, Y. S.; Li, S.; He, M. Z.; Zhang, F.; Feng, X. L. Self-Assembled Fe_2O_3/Graphene Aerogel with High Lithium Storage Performance. *ACS Appl. Mater. Interfaces* **2013**, *5*, 3764−3769.

(17) Wei, W.; Yang, S. B.; Zhou, H. X.; Lieberwirth, I.; Feng, X. L.; Müllen, K. 3D Graphene Foams Cross-linked with Pre-Encapsulated Fe_3O_4 Nanospheres for Enhanced Lithium Storage. *Adv. Mater.* **2013**, *22*, 2909−2914.

(18) Gong, Y. J.; Yang, S. B.; Zhan, L.; Ma, L. L.; Vajtai, R.; Ajayan, P. M. A Bottom-Up Approach To Build 3D Architectures from Nanosheets for Superior Lithium Storage. *Adv. Funct. Mater.* **2014**, *24*, 125−130.

(19) Luo, J.; Liu, J.; Zeng, Z.; Ng, C. F.; Ma, L.; Zhang, H.; Lin, J.; Shen, Z.; Fan, H. J. Three-Dimensional Graphene Foam Supported Fe_3O_4 Lithium Battery Anodes with Long Cycle Life and High Rate Capability. *Nano Lett.* **2013**, *13*, 6136−6143.

(20) Chen, W. F.; Li, S. R.; Chen, C. H.; Yan, L. F. Self-Assembly and Embedding of Nanoparticles by In Situ Reduced Graphene for Preparation of a 3D Graphene/Nanoparticle Aerogel. *Adv. Mater.* **2011**, *23*, 5679−5683.

(21) Cong, H. P.; Ren, X. C.; Wang, P.; Yu, S. H. Macroscopic Multifunctional Graphene-Based Hydrogels and Aerogels by a Metal Ion Induced Self-Assembly Process. *ACS Nano* **2012**, *6*, 2693−2703.

(22) Gong, Y. J.; Yang, S. B.; Liu, Z.; Ma, L. L.; Vajtai, R.; Ajayan, P. M. Graphene-Network-Backboned Architectures for High-Performance Lithium Storage. *Adv. Mater.* **2013**, *25*, 3979−3984.

(23) Zhang, H.; Xie, A. J.; Wang, C. P.; Wang, H. S.; Shen, Y. H.; Tian, X. Y. Novel rGO/α-Fe_2O_3 Composite Hydrogel: Synthesis, Characterization and High Performance of Electromagnetic Wave Absorption. *J. Mater. Chem. A* **2013**, *1*, 8547−8553.

(24) Zhang, Z. Y.; Xiao, F.; Guo, Y. L.; Wang, S.; Liu, Y. Q. One-Pot Self-Assembled Three-Dimensional TiO_2-Graphene Hydrogel with Improved Adsorption Capacities and Photocatalytic and Electrochemical Activities. *ACS Appl. Mater. Interfaces* **2013**, *5*, 2227−2233.

(25) Li, B.; Cao, H.; Zhang, J.; Qu, M.; Lian, F.; Kong, X. SnO_2-Carbon-RGO Heterogeneous Electrode Materials with Enhanced Anode Performances in Lithium Ion Batteries. *J. Mater. Chem.* **2012**, *22*, 2851−2854.

(26) Parvez, K.; Yang, S.; Hernandez, Y.; Winter, A.; Turchanin, A.; Feng, X.; Müllen, K. Nitrogen-Doped Graphene and Its Iron-Based Composite As Efficient Electrocatalysts for Oxygen Reduction Reaction. *ACS Nano* **2012**, *6*, 9541−9550.

(27) Zhou, X.; Bao, J.; Dai, Z.; Guo, Y.-G. Tin Nanoparticles Impregnated in Nitrogen-Doped Graphene for Lithium-Ion Battery Anodes. *J. Phys. Chem. C* **2013**, *117*, 25367−25373.

(28) Vinayan, B. P.; Ramaprabhu, S. Facile Synthesis of SnO_2 Nanoparticles Dispersed Nitrogen Doped Graphene Anode Material for Ultrahigh Capacity Lithium Ion Battery Applications. *J. Mater. Chem. A* **2013**, *1*, 3865−3871.
(29) Du, M.; Xu, C. H.; Sun, J.; Gao, L. One Step Synthesis of Fe_2O_3/Nitrogen-Doped Graphene Composite As Anode Materials for Lithium Ion Batteries. *Electrochim. Acta* **2012**, *80*, 302−307.
(30) Cai, D. D.; Li, D. D.; Wang, S. Q.; Zhu, X. F.; Yang, W. S.; Zhang, S. Q.; Wang, H. H. High Rate Capability of TiO_2/Nitrogen-Doped Graphene Nanocomposite As an Anode Material for Lithium-Ion Batteries. *J. Alloys. Compd.* **2013**, *561*, 54−58.
(31) Li, D.; Shi, D. Q.; Liu, Z. W.; Liu, H. K.; Guo, Z. P. TiO_2 Nanoparticles on Nitrogen-Doped Graphene As Anode Material for Lithium Ion Batteries. *J. Nanopart. Res.* **2013**, *15*, 1674−1683.
(32) Zhang, K. J.; Han, P. X.; Gu, L.; Zhang, L. X.; Liu, Z. H.; Kong, Q. S.; Zhang, C. J.; Dong, S. M.; Zhang, Z. Y.; Yao, J. H.; Xu, H. X.; Cui, G. L.; Chen, L. Q. Synthesis of Nitrogen-Doped MnO/Graphene Nanosheets Hybrid Material for Lithium Ion Batteries. *ACS Appl. Mater. Interfaces* **2012**, *4*, 658−664.
(33) Li, D.; Shi, D. Q.; Chen, Z. X.; Liu, H. K.; Jia, D. Z.; Guo, Z. P. Enhanced Rate Performance of Cobalt Oxide/Nitrogen Doped Graphene Composite for Lithium Ion Batteries. *RSC Adv.* **2013**, *3*, 5003−5008.
(34) Zhou, X. S.; Wan, L. J.; Guo, Y. G. Binding SnO^2 Nanocrystals in Nitrogen-Doped Graphene Sheets as Anode Materials for Lithium-Ion Batteries. *Adv. Mater.* **2013**, *25*, 2152−2157.
(35) Xu, C. H.; Sun, J.; Gao, L. Controllable Synthesis of Monodisperse Ultrathin SnO_2 Nanorods on Nitrogen-Doped Graphene and Its Ultrahigh Lithium Storage Properties. *Nanoscale* **2012**, *4*, 5425−5430.
(36) Chang, Y.; Li, J.; Wang, B.; Luo, H.; He, H.; Song, Q.; Zhi, L. Synthesis of 3D Nitrogen-Doped Graphene /Fe_3O_4 by a Metal Ion Induced Self-Assembly Process for High-Performance Li-Ion Batteries. *J. Mater. Chem. A* **2013**, *1*, 14658−14665.
(37) Lian, P. C.; Zhu, X. F.; Liang, S. Z.; Li, Z.; Yang, W. S.; Wang, H. H. High Reversible Capacity of SnO_2/Graphene Nanocomposite As an Anode Material for Lithium-Ion Batteries. *Electrochim. Acta* **2011**, *56*, 4532−4539.
(38) Huang, Y. S.; Wu, D. Q.; Han, S.; Li, S.; Xiao, L.; Zhang, F.; Feng, X. L. Assembly of Tin Oxide/Graphene Nanosheets into 3D Hierarchical Frameworks for High-Performance Lithium Storage. *ChemSusChem* **2013**, *6*, 1510−1515.
(39) Kim, C.; Noh, M.; Choi, M.; Cho, J.; Park, B. Critical Size of a Nano SnO_2 Electrode for Li-Secondary Battery. *Chem. Mater.* **2005**, *17*, 3297−3301.
(40) Gregory, J. Basic Principles of Colloid Science - Everett, D. H. *Nature* **1989**, *338*, 182−182.
(41) Wang, R. H.; Wang, Y.; Xu, C. H.; Sun, J.; Gao, L. Facile One-Step Hydrazine-Assisted Solvothermal Synthesis of Nitrogen-Doped Reduced Graphene Oxide: Reduction Effect and Mechanisms. *RSC Adv.* **2013**, *3*, 1194−1200.
(42) Zhou, D.; Cheng, Q.-Y.; Han, B.-H. Solvothermal Synthesis of Homogeneous Graphene Dispersion with High Concentration. *Carbon* **2011**, *49*, 3920−3927.
(43) Reddy, A. L. M.; Srivastava, A.; Gowda, S. R.; Gullapalli, H.; Dubey, M.; Ajayan, P. M. Synthesis of Nitrogen-Doped Graphene Films for Lithium Battery Application. *ACS Nano* **2010**, *4*, 6337−6342.
(44) Yu, Y. X. Can All Nitrogen-Doped Defects Improve the Performance of Graphene Anode Materials for Lithium-Ion Batteries? *Phys. Chem. Chem. Phys.* **2013**, *15*, 16819−16827.
(45) Jiang, Y. Z.; Yuan, T. Z.; Sun, W. P.; Yan, M. Electrostatic Spray Deposition of Porous SnO_2/Graphene Anode Films and Their Enhanced Lithium-Storage Properties. *ACS Appl. Mater. Interfaces* **2012**, *4*, 6216−6220.
(46) Jiang, S. H.; Yue, W. B.; Gao, Z. Q.; Ren, Y.; Ma, H.; Zhao, X. H.; Liu, Y. L.; Yang, X. J. Graphene-Encapsulated Mesoporous SnO_2 Composites As High Performance Anodes for Lithium-Ion Batteries. *J. Mater. Sci.* **2013**, *48*, 3870−3876.
(47) Wang, B.; Su, D. W.; Park, J.; Ahn, H.; Wang, G. X. Graphene-Supported SnO_2 Nanoparticles Prepared by a Solvothermal Approach for an Enhanced Electrochemical Performance in Lithium-Ion Batteries. *Nanoscale Res. Lett.* **2012**, *7*, 215.
(48) Song, H. W.; Li, N.; Cui, H.; Wang, C. X. Enhanced Capability and Cyclability of SnO_2-Graphene Oxide Hybrid Anode by Firmly Anchored SnO_2 Quantum Dots. *J. Mater. Chem. A* **2013**, *1*, 7558−7562.
(49) Wang, D. N.; Yang, J. L.; Li, X. F.; Geng, D. S.; Li, R. Y.; Cai, M.; Sham, T.-K.; Sun, X. L. Layer by Layer Assembly of Sandwiched Graphene/SnO_2 Nanorod/Carbon Nanostructures with Ultrahigh Lithium Ion Storage Properties. *Energy Environ. Sci.* **2013**, *6*, 2900−2906.
(50) Zhang, L. S.; Jiang, L. Y.; Yan, H. J.; Wang, W. D.; Wang, W.; Song, W. G.; Guo, Y. G.; Wan, L. J. Monodispersed SnO_2 Nanoparticles on Both Sides of Single Layer Graphene Sheets As Anode Materials in Li-Ion Batteries. *J. Mater. Chem.* **2010**, *20*, 5462−5467.
(51) Wang, G.; Wang, B.; Wang, X.; Park, J.; Dou, S.; Ahn, H.; Kim, K. Sn/Graphene Nanocomposite with 3D Architecture for Enhanced Reversible Lithium Storage in Lithium Ion Batteries. *J. Mater. Chem.* **2009**, *19*, 8378−8384.
(52) Han, X.; Qing, G.; Sun, J.; Sun, T. How Many Lithium Ions Can Be Inserted onto Fused C6 Aromatic Ring Systems? *Angew. Chem., Int. Ed.* **2012**, *51*, 5147−5151.
(53) Zhang, H.-X.; Feng, C.; Zhai, Y.-C.; Jiang, K.-L.; Li, Q.-Q.; Fan, S.-S. Cross-Stacked Carbon Nanotube Sheets Uniformly Loaded with SnO_2 Nanoparticles: A Novel Binder-Free and High-Capacity Anode Material for Lithium-Ion Batteries. *Adv. Mater.* **2009**, *21*, 2299−2304.
(54) Xin, S.; Guo, Y.-G.; Wan, L.-J. Nanocarbon Networks for Advanced Rechargeable Lithium Batteries. *Acc. Chem. Res.* **2012**, *45*, 1759−1769.
(55) Wu, X.-L.; Jiang, L.-Y.; Cao, F.-F.; Guo, Y.-G.; Wan, L.-J. $LiFePO_4$ Nanoparticles Embedded in a Nanoporous Carbon Matrix: Superior Cathode Material for Electrochemical Energy-Storage Devices. *Adv. Mater.* **2009**, *21*, 2710−2714.
(56) Jamnik, J.; Maier, J. Nanocrystallinity Effects in Lithium Battery Materials Aspects of Nano-Ionics. Part IV. *Phys. Chem. Chem. Phys.* **2003**, *5*, 5215−5220.
(57) Guo, Y. G.; Zhou, X. S.; Yin, Y. X.; Wan, L. J. A Robust Composite of SnO_2 Hollow Nanospheres Enwrapped by Graphene As High-Capacity Anode Materials for Lithium-Ion Batteries. *J. Mater. Chem.* **2012**, *22*, 17456−17459.
(58) Luo, B.; Wang, B.; Li, X. L.; Jia, Y. Y.; Liang, M. H.; Zhi, L. J. Graphene-Confined Sn Nanosheets with Enhanced Lithium Storage Capability. *Adv. Mater.* **2012**, *24*, 3538−3543.
(59) He, M.; Yuan, L. X.; Hu, X.; Zhang, W.; Shu, J.; Huang, Y. SnO_2@Carbon Nanocluster Anode Material with Superior Cyclability and Rate Capability for Lithium-Ion Batteries. *Nanoscale* **2013**, *5*, 3298−3305.
(60) Li, X. F.; Meng, X. B.; Liu, J.; Geng, D. S.; Zhang, Y.; Banis, M. N.; Li, Y. L.; Yang, J. L.; Li, R. Y.; Sun, X. L.; Cai, M.; Verbrugge, M. W. Tin Oxide with Controlled Morphology and Crystallinity by Atomic Layer Deposition onto Graphene Nanosheets for Enhanced Lithium Storage. *Adv. Funct. Mater.* **2012**, *22*, 1647−1654.
(61) Liang, J. F.; Zhao, Y.; Guo, L.; Li, L. D. Flexible Free-Standing Graphene/SnO_2 Nanocomposites Paper for Li-Ion Battery. *ACS Appl. Mater. Interfaces* **2012**, *4*, 5742−5748.
(62) Wang, J. Z.; Lu, L.; Lotya, M.; Coleman, J. N.; Chou, S. L.; Liu, H. K.; Minett, A. I.; Chen, J. Development of MoS_2−CNT Composite Thin Film from Layered MoS_2 for Lithium Batteries. *Adv. Energy Mater.* **2013**, *3*, 798−805.
(63) Chan, C. K.; Ruffo, R.; Hong, S. S.; Cui, Y. Surface Chemistry and Morphology of the Solid Electrolyte Interphase on Silicon Nanowire Lithium-Ion Battery Anodes. *J. Power Sources* **2009**, *189*, 1132−1140.
(64) Wang, C.; Appleby, A. J.; Little, F. E. Charge−Discharge Stability of Graphite Anodes for Lithium-Ion Batteries. *J. Electroanal. Chem.* **2001**, *497*, 33−46.

(65) Zhong, C.; Wang, J. Z.; Chen, Z. X.; Liu, H. K. SnO_2-Graphene Composite Synthesized via an Ultrafast and Environmentally Friendly Microwave Autoclave Method and Its Use As a Superior Anode for Lithium-Ion Batteries. *J. Phys. Chem. C* **2011**, *115*, 25115−25120.